

## How to make GaMnAs with a high ferromagnetic phase transition temperature?

J. SADOWSKI<sup>1,2\*</sup>, J. Z. DOMAGAŁA<sup>1</sup>, J. KANSKI<sup>3</sup>,  
C. H. RODRIGUEZ<sup>4</sup>, F. TERKI<sup>4</sup>, S. CHARAR<sup>4</sup>, D. MAUDE<sup>5</sup>

<sup>1</sup>Institute of Physics, Polish Academy of Sciences, al. Lotników 32/46, 02-668 Warszawa, Poland

<sup>2</sup>Institut für Angewandte und Experimentelle Physik, Universität Regensburg,  
93040 Regensburg, Germany

<sup>3</sup>Department of Applied Physics, Chalmers University of Technology, SE-41296 Göteborg, Sweden

<sup>4</sup>Groupe d'Etude des Semiconducteurs CC074, Université Montpellier II, Montpellier, France

<sup>5</sup>High Magnetic Field Laboratory, CNRS-MPI, 25 Avenue des Martyrs, 38042 Grenoble, France

We analyse the role of structural defects in GaMnAs and demonstrate how their density can be drastically reduced by *in situ* post-growth annealing under As capping. Modifications of the magnetic, transport, and structural properties of annealed GaMnAs layers are presented. The main result is that Curie temperatures are strongly increased relative to those of as-grown layers, typically from 70–80 K to 150–160 K. The annealed layers exhibit well-ordered smooth surfaces, suitable for further epitaxial overgrowth.

Key words: *ferromagnetic semiconductor; molecular beam epitaxy; defect, annealing*

### 1. Introduction

GaMnAs is a model semiconductor with carrier-induced ferromagnetism. It is currently being used to test prototype spintronic devices, such as spin-diodes [1] and giant magnetoresistance structures [2]. Since the first report on ferromagnetism in GaMnAs by Ohno et al. [3], a lot of interesting, spin-related phenomena have been observed in this material. The remarkable magnetotransport properties of GaMnAs enabled the observation of the giant planar Hall effect [4], current driven magnetization reversal [5], and the dependence of magnetic anisotropy on the concentration of carriers [6]. In spite of these results associated with the magnetic properties of GaMnAs, it is still desirable to improve its quality and obtain a material with the ferromagnetic phase transition temperature ( $T_c$ ) significantly higher than the present record value of 173 K. The mean field Zener model of carrier-

---

\*Corresponding author, e-mail: sadow@ifpan.edu.pl

mediated ferromagnetism in transition metal doped semiconductors developed by Dietl et al. [7] predicts that  $T_c$  will reach room temperature for GaMnAs containing 10% of Mn [8] and correspondingly high concentrations of carriers (valence band holes).

The presence of valence band holes is indeed underlined by recently reported extraordinarily high  $T_c$  values (250 K) in delta-doped AlGaAs/GaAs quantum well structures [9]. This is also the underlying reason for the markedly increased  $T_c$  values accompanying post-growth annealing discussed here. The direct effect of annealing is the efficient removal of Mn atoms from interstitial positions ( $Mn_i$ ). As shown both theoretically [10, 11] and experimentally, these defects are always present in as-grown GaMnAs, with concentrations of up to about 20% of total Mn content, and they act as double donors. Thus, by reducing the density of Mn interstitials, the density of valence band holes is expected to increase. This was first demonstrated by Edmonds et al. [12], who found that  $Mn_i$  defects can be removed by low temperature post-growth annealing of samples exposed to the air after MBE growth. Since GaMnAs with Mn concentrations in the range of a few at. % is intrinsically metastable, the annealing temperature should be kept low. At temperatures above 300 °C, GaMnAs starts to decompose to MnAs inclusions in a GaAs matrix. These inclusions, if sufficiently large, are also ferromagnetic, since MnAs is a ferromagnetic metal with  $T_c = 40$  °C, but the GaAs:MnAs system is usually highly resistive, and the main advantage of GaMnAs, namely ferromagnetism mediated by carriers in a semiconductor, is lost. The best results achieved so far are thus obtained after very long annealing periods (~100 hours) at temperatures well below the growth temperature [12]. Higher annealing temperatures and short annealing times (0.5–3 hrs) have also been successfully applied [13–15].

In this paper, we present a modification of the low-temperature annealing method, which uses amorphous As layers deposited on the GaMnAs surface directly after MBE growth as a passivating medium for out-diffused Mn interstitials. We show that our method is more efficient in terms of shorter annealing times and lower annealing temperatures than annealing in air. Moreover, it leaves the GaMnAs surface suitable for further epitaxy, either in the same MBE system which was used for GaMnAs layer growth, or in another MBE system, since As capping forms a protective layer inhibiting surface oxidation and preserving a clean, atomically flat, as-grown surface.

## 2. Sample preparation

GaMnAs samples were grown in a KRYOVAK MBE system, located at MAX-Lab, Lund University, Sweden. Arsenic was supplied from a valved cracker source. The epi-ready GaAs(100) substrates were attached to molybdenum holders with liquid In. After thermal desorption of the native oxide, a standard high temperature GaAs buffer was deposited. The substrate temperature was then decreased to 230–240 °C for growing the GaMnAs layer. During this growth, the  $As_2$  to Ga flux ratio was about 2, and the growth rate about 0.2 molecular layers (ML) per second. The growth was

monitored by reflection high-energy electron diffraction (RHEED). The diffraction showed a 2-dimensional monocrystalline GaMnAs surface, with (1×2) surface reconstruction, and no admixture of other phases (such as MnAs inclusions). Intensity oscillations of the specular beam were used to measure GaMnAs composition *in-situ*, by measuring the growth rate increase of GaMnAs with respect to GaAs. The thicknesses of the GaMnAs layers were chosen between 100 and 1000 Å (thicker layers usually exhibit worse magnetic properties). After completing GaMnAs growth, the As flux was cut by closing the As shutter as well as the As-cracker valve. The substrate heater was then turned off, and when the temperature fell below 150 °C, the As valve and shutter were open again for depositing a thick amorphous As layer. The thickness of this capping layer was in the range 1000 – 2000 Å, as measured by SIMS.

### 3. Defects in GaMnAs

The most abundant defects present in GaMnAs are As antisites ( $\text{As}_{\text{Ga}}$ ) and Mn interstitials. Both defects are double donors, effectively compensating the p-doping provided by Mn atoms in Ga sites ( $\text{Mn}_{\text{Ga}}$ ). In the Zener mean field model [7],  $T_c$  depends on the density of local moments and the density of charge carriers according to the relation

$$T_c \sim [\text{Mn}_{\text{Ga}}]p^{1/3} \quad (1)$$

Due to the compensating effect of  $\text{As}_{\text{Ga}}$  and  $\text{Mn}_{\text{I}}$  defects, the net density of holes  $p$  is

$$p = [\text{Mn}_{\text{Ga}}] - 2([\text{As}_{\text{Ga}}] + [\text{Mn}_{\text{I}}]) \quad (2)$$

According to (1) and (2), maximising  $T_c$  requires both a maximum concentration of  $\text{Mn}_{\text{Ga}}$  and minimum concentration of  $\text{As}_{\text{Ga}}$  and  $\text{Mn}_{\text{I}}$  defects. These two demands are in effect contradictory, since increasing Mn content in GaMnAs requires a reduced growth temperature [16, 17]. Low growth temperature, however, promotes the formation of As antisite defects [18]. Thus, there exists a Mn concentration that provides compromise between these two tendencies. Experimental evidence suggests that this optimum Mn content is in the range 6–8 at. %. The maximum Mn content achieved so far in uniform GaMnAs is 10% [19], however growing  $\text{Ga}_{0.94}\text{Mn}_{0.06}\text{As}$  requires very low growth temperatures (about 150 °C) and special growth procedures. The concentrations of two compensating defects ( $\text{As}_{\text{Ga}}$  and  $\text{Mn}_{\text{I}}$ ) can attain levels [20, 21] of ca. 0.5 and 1.7 at. %, respectively, which means that the compensation degree in GaMnAs can be as high as 50–70%. Indeed, such high compensation levels are observed in the as-grown material. As an example we show in Fig. 1 the results of the Hall effect measurements for a 300 Å thick  $\text{Ga}_{0.94}\text{Mn}_{0.06}\text{As}$  layer. A general problem in extracting carrier concentration in GaMnAs from the Hall effect measurements is negative magnetoresistance, which can be quite large, up to 20–30%. In the case of the sample shown in Fig. 1, the negative magnetoresistance is rather small, only about 2%. In this case, the value of  $p$  can be taken from the  $R_{xy}$  vs.  $B$  slope without the necessity of sub-

tracting the negative magnetoresistance, and we thus find  $p = 6.5 \times 10^{20} \text{ cm}^{-3}$ . Mn content of 6% should provide a hole density of  $1.32 \times 10^{21} \text{ cm}^{-3}$ , which means that the compensation of  $\text{Mn}_{\text{Ga}}$  in this sample is on the level of 50%. This compensation is due to both  $\text{As}_{\text{Ga}}$  and  $\text{Mn}_{\text{I}}$ , and it is not possible to estimate their individual contributions without additional measurements.

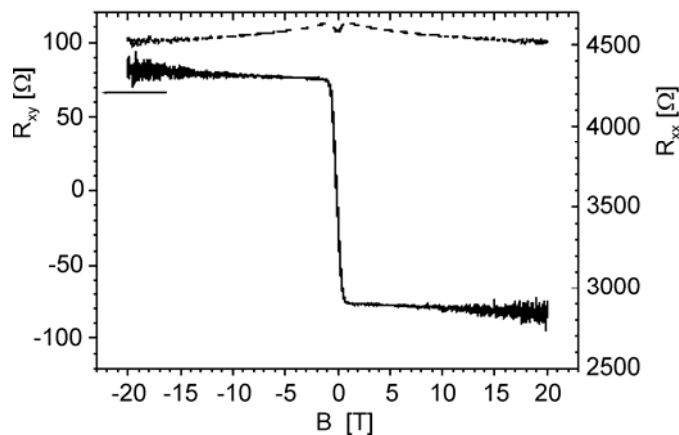


Fig. 1. Results of Hall effect measurements for an as-grown 300 Å thick  $\text{Ga}_{0.94}\text{Mn}_{0.06}\text{As}$  layer. Solid curve – Hall resistance  $R_{xy}$ , dashed curve – longitudinal resistance  $R_{xx}$ . The concentration of holes in the sample –  $6.5 \times 10^{20} \text{ cm}^{-3}$  (50% compensation of  $\text{Mn}_{\text{Ga}}$  acceptors)

The concentration of  $\text{Mn}_{\text{I}}$  can be obtained from Rutherford back-scattering (RBS) and particle-induced X-ray emission (PIXE) measurements [21] but the density of  $\text{As}_{\text{Ga}}$  in GaMnAs is more difficult to assess. Since the density of As antisites is mainly related to the growth temperature, and it is independent of the presence of Mn interstitials [22], one can expect that the concentration of  $\text{As}_{\text{Ga}}$  in GaMnAs should be the same as in GaAs grown at the same low temperature. In the case of LT GaAs, the density of  $\text{As}_{\text{Ga}}$  defects can be determined by X-ray diffraction (XRD), since these defects cause a crystal lattice expansion proportional to their content [18, 23] (in the case of GaMnAs the situation is more complicated, since both  $\text{As}_{\text{Ga}}$  and  $\text{Mn}_{\text{I}}$  cause lattice expansion). Thus, by measuring XRD on the LT-GaAs buffer layers grown prior to GaMnAs, we can estimate the density of As antisites. Fig. 2 shows the results of XRD measurements for three 500 Å thick  $\text{Ga}_{0.96}\text{Mn}_{0.04}\text{As}$  samples grown at conditions that change the concentration of  $\text{As}_{\text{Ga}}$ , namely at different  $\text{As}_2/\text{Ga}$  flux ratios (2, 5, and 9). The inset shows a comparison between the measured and calculated XRD spectra for the sample with the lowest  $\text{As}_2/\text{Ga}$  flux ratio. The presence of X-ray interference fringes in the measured curve and a very good correspondence between the measured and calculated spectra prove a high quality of the GaMnAs layers – the broadening of the GaMnAs peaks is due to small film thickness. In these curves, the contribution from the LT-GaAs buffer layer is seen as a shoulder on the low-angle

side of the main (004) peak of the GaAs substrate. It is clear that the sample grown at the lowest  $\text{As}_2/\text{Ga}$  flux ratio has also the lowest  $\text{As}_{\text{Ga}}$  concentration, since the shoulder is least pronounced in this case.

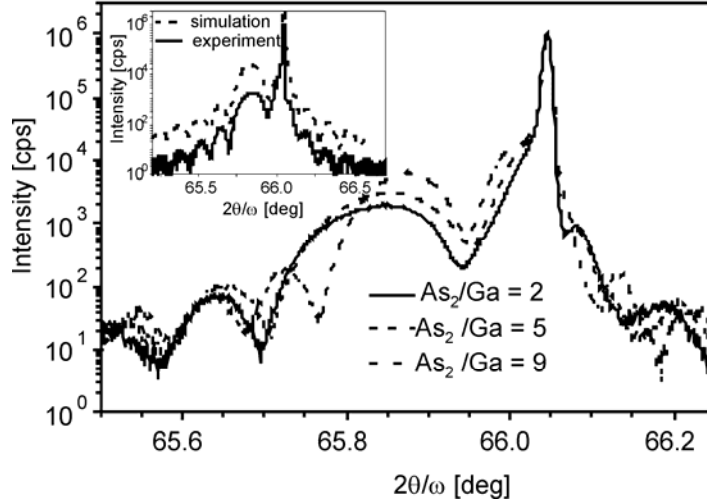


Fig. 2. (004) X-ray Bragg reflections for three 500 Å thick  $\text{Ga}_{0.96}\text{Mn}_{0.04}\text{As}$  samples grown at different  $\text{As}_2/\text{Ga}$  flux ratios. The highest intensity peak on the right side results from diffraction on the GaAs(001) substrate. Broad peaks at lower angles are due to diffraction on GaMnAs layers. The inset shows a comparison between simulated and measured spectra for the sample grown at the lowest  $\text{As}_2/\text{Ga}$  flux ratio

For samples grown at higher  $\text{As}_2/\text{Ga}$  flux ratios, the peaks from LT-GaAs are shifted further towards lower diffraction angles, reflecting a lattice expansion caused by the  $\text{As}_{\text{Ga}}$  defects. In contrast, the diffraction peaks from the GaMnAs layers shift towards higher angles for increasing  $\text{As}_2/\text{Ga}$  flux ratios. This suggests that the concentration of  $\text{Mn}_{\text{I}}$  decreases with an increasing concentration of  $\text{As}_{\text{Ga}}$  in GaMnAs. The quantitative analysis of this process has been presented elsewhere [23].

#### 4. Defect removal by post-growth annealing

From the two defects considered above, namely As antisites and Mn interstitials, the latter is only weakly bound, and can be effectively removed from the GaMnAs bulk by post-growth annealing [12–15, 24]. It has been also shown [24, 25–28] that the essential factor in post-growth annealing is the surface passivation of the out-diffused  $\text{Mn}_{\text{I}}$  atoms. The annealing of GaMnAs layers capped with even very thin LT GaAs films was found to be ineffective [25]. Moreover, the annealing efficiency of GaMnAs layers with rough surfaces was found to be enhanced compared to smooth layers [28]. All these results suggest that post-growth annealing is associated with pas-

sivating the diffusing  $Mn_I$  defects at the GaMnAs surface. Passivation can be due to chemical bonding with oxygen or nitrogen when the GaMnAs surface is exposed to air, or with another reactive element that can be deposited on the GaMnAs surface after MBE growth. We have recently proposed to use an amorphous As capping as a passivating species [24], and all the annealing results presented here concern this situation.

Figure 3 presents the results of the Hall effect measurements for the same sample as in Fig. 1, but after post growth annealing performed at 180 °C for 3 hours. The removal efficiency of Mn interstitials is close to 100%, since the concentration of holes increased from  $6.5 \times 10^{21} \text{ cm}^{-3}$  to  $1.3 \times 10^{21} \text{ cm}^{-3}$ , which corresponds almost exactly to the content of  $Mn_{Ga}$ . The ferromagnetic phase transition temperature for this sample is 150 K.

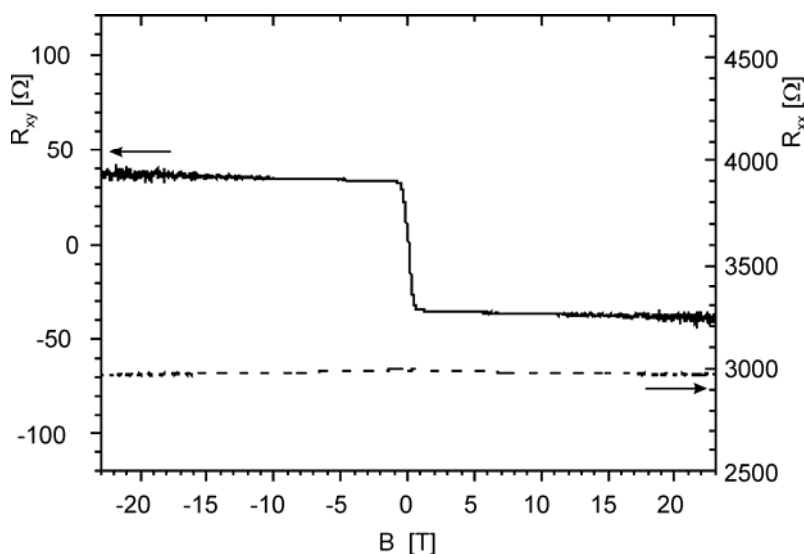


Fig. 3. Results of Hall effect measurements for a 300 Å thick  $Ga_{0.94}Mn_{0.06}As$  layer annealed for 3h at 180 °C. Solid curve – hall resistance  $R_{xy}$ , dashed curve – longitudinal resistance  $R_{xx}$ .

The concentration of holes in the sample is  $1.3 \times 10^{21} \text{ cm}^{-3}$ , corresponding almost exactly to the content of Mn at Ga sites (Mn interstitial defects effectively removed by post-growth annealing). The scales for  $R_{xx}$  and  $R_{xy}$  are the same as in Fig. 1

Figure 4 shows the temperature dependence of magnetization, measured by a SQUID magnetometer for a 400 Å thick  $Ga_{0.94}Mn_{0.06}As$  layer with amorphous As capping, before and after annealing at 180 °C for 2h. This sample is very similar to the one in Fig. 3, but somewhat thicker. The remarkable increase of  $T_c$  from about 70 K to about 150 K can also be seen for this sample. The  $T_c$  increase is correlated with the increased saturation magnetisation observed at low temperatures. This is due to the removal of antiferromagnetically coupled pairs of  $Mn_{Ga}-Mn_I$ , which are excluded from participating in the FM phase of the non-annealed sample.

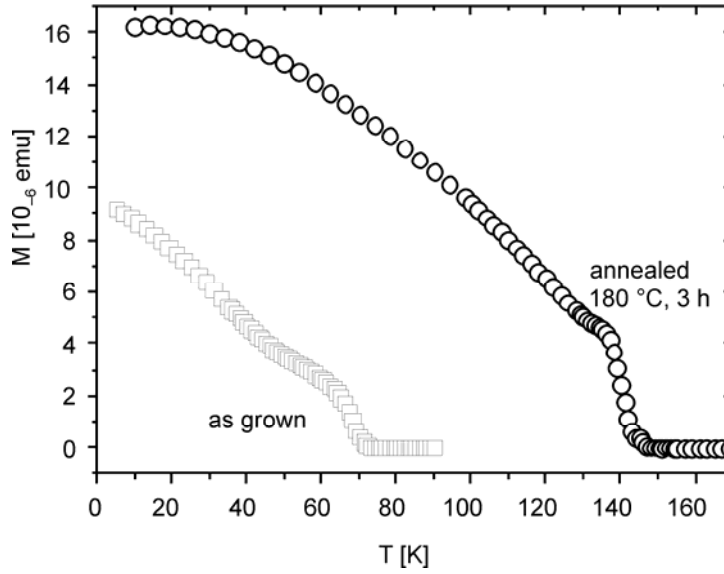


Fig. 4. Temperature dependence of magnetization for a 400 Å thick  $\text{Ga}_{0.94}\text{Mn}_{0.06}\text{As}$  layer with an amorphous As capping surface layer, before and after post-growth annealing at 180 °C for 3h. Post-growth annealing increases both  $T_c$  and the saturation magnetization

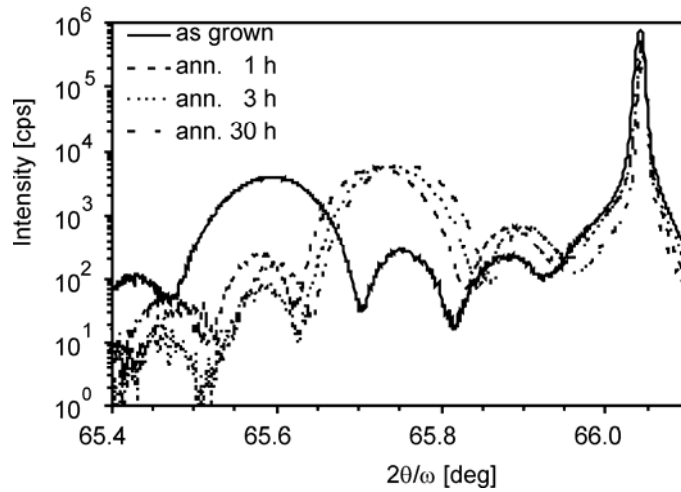


Fig. 5. (004) X-ray Bragg reflections for not annealed (solid curve) and annealed pieces of As-capped 700 Å thick  $\text{Ga}_{0.94}\text{Mn}_{0.06}\text{As}$  layers. The shifts in the GaMnAs diffraction peaks to higher angles upon annealing are due to the annealing-induced reduction of the GaMnAs lattice parameter

The efficiency of removing  $\text{Mn}_i$  defects by annealing As-capped samples is also confirmed by XRD measurements (see Fig. 5). As already discussed, Mn interstitials cause lattice expansion, so that the lattice constant is expected to decrease upon removing these defects. Figure 5 shows significant shifts of (004) Bragg reflections

from a 700 Å thick  $\text{Ga}_{0.94}\text{Mn}_{0.06}\text{As}$  layer after consecutive annealings lasting 1, 2, 3, and 30 hrs at 180 °C. Already after 1 hour of annealing the GaMnAs lattice parameter is significantly reduced, annealing for 2 and 3 hours induce only small further reductions, and annealing for further 30 hours has no effect.

## 5. Conclusions

An efficient method for eliminating Mn interstitials from GaMnAs by post-growth annealing under As capping has been demonstrated. The efficiency of the process is proved by a significant increase of  $T_c$ , up to 150 K, for  $\text{Ga}_{0.94}\text{Mn}_{0.06}\text{As}$ , as well as by an increase in the concentration of holes to the range of  $10^{21} \text{ cm}^{-3}$ . An additional advantage of our method is that the treatment is carried out *in situ*, and that the surfaces of the annealed layers are smooth and well-ordered. This provides possibility of performing further epitaxial growth on top of the high quality, Mn interstitial-defect-free GaMnAs layers.

## Acknowledgements

The present work is part of a project supported by the Swedish Research Council VR. One of the authors (J.S.) acknowledges the financial support from the Polish State Committee for Scientific Research (KBN) through Grant No. PBZ-KBN-044/P03/2001. Measurements at high magnetic fields were supported by the European Community within the *Access to Research Infrastructure action of the Improving Human Potential Programme*.

## References

- [1] FLATTÉ M.E., VIGNALE G., Appl. Phys. Lett., 78 (2001), 1273.
- [2] MATTANA R., ELSÉN M., GEORGE J.-M., JAFFRÈS H., NGUYEN VAN DAU F., FERT A., WYCZISK M.F., OLIVIER J., GALTIER P., LÉPINE B., GUIVARC'H A., JÉZÉQUEL G., Phys. Rev. B, 71 (2005), 075206.
- [3] OHNO H., SHEN A., MATSUKURA F., OIWA A., ENDO A., KATSUMOTO S., IYE Y., Appl. Phys. Lett., 69 (1996), 363.
- [4] TANG H.X., KAWAKAMI R.K., AWSCHALOM D.D., ROUKES M.L., Phys. Rev. Lett., 90 (2003), 107201.
- [5] CHIBA D., SATO Y., KITA T., MATSUKURA F., OHNO H., Phys. Rev. Lett., 93 (2004), 216602.
- [6] SAWICKI M., WANG K.-Y., EDMONDS K.W., CAMPION R.P., STADDON C.R., FARLEY N.R.S., FOXON C.T., PAPIŚ E., KAMINSKA E., PIOTROWSKA A., DIETL T., GALLAGHER B.L., Phys. Rev. B, 71 (2005), 121302.
- [7] DIETL T., OHNO H., MATSUKURA F., Phys. Rev. B, 63 (2001), 195205.
- [8] DIETL T., Semicond. Sci. Technol., 17 (2002), 377.
- [9] NAZMUL A.M., AMEMIYA T., SHUTO Y., SUGAHARA S., TANAKA M., Phys. Rev. Lett., 95 (2005), 017201.
- [10] MASEK J., MACA F., Acta Phys. Polon. A, 100 (2001), 319.
- [11] BLINOWSKI J., KACMAN P., Phys. Rev. B, 67 (2003), 121204.
- [12] EDMONDS K.W., BOGUSŁAWSKI P., WANG K.Y., CAMPION R.P., NOVIKOV S.N., FARLEY N.R.S., GALLAGHER B.L., FOXON C.T., SAWICKI M., DIETL T., BUONGIORNO NARDELLI M., BERNHOLC J., Phys. Rev. Lett., 92 (2004), 037201.
- [13] CHIBA D., TAKAMURA K., MATSUKURA F., OHNO H., Appl. Phys. Lett., 82 (2003), 3020.



- [14] KU K.C., POTASHNIK S.J., WANG R.F., CHUN S.H., SCHIFFER P., SAMARTH N., SEONG M.J., MASCARENHAS A., JOHNSTON-HALPERIN E., MYERS R.C., GOSSARD A.C., AWSCHALOM D.D., *Appl. Phys. Lett.*, **82** (2003), 2302.
- [15] KIRBY B.J., BORCHERS J.A., RHYNE J.J., TE VELTHUIS S.G.E., HOFFMANN A., O'DONOVAN K.V., WOJTOWICZ T., LIU X., LIM W.L., FURDYNA J.K., *Phys. Rev. B*, **69** (2004), 081307.
- [16] OHNO H., *Science*, **281** (1998), 951.
- [17] SADOWSKI J., DOMAGALA J.Z., BAK-MISIUK J., KOLESNIK S., SAWICKI M., SWIATEK K., KANSKI J., ILVER L., STRÖM V., *J. Vac. Sci. Technol. B*, **18** (2000), 1697.
- [18] LIU X., PRASAD A., NISHIO J., WEBER E.R., LILIENTAL-WEBER Z., WALUKIEWICZ W., *Appl. Phys. Lett.*, **67** (1995), 279.
- [19] SADOWSKI J., MATHIEU R., SVEDLINDH P., DOMAGALA J.Z., BAK-MISIUK J., SWIATEK K., KARLSTEEN M., KANSKI J., ILVER L., ÅSKLUND H., SÖDERVALL U., *Appl. Phys. Lett.*, **78** (2001), 3271.
- [20] STAAB T.E.M., NIEMINEN R.M., GEBAUER J., KRAUSE-REHBERG R., LUYSBERG M., HAUGK, M., FRAUENHEIM TH., *Phys. Rev. Lett.*, **87** (2001), 045504.
- [21] YU K.M., WALUKIEWICZ W., WOJTOWICZ T., KURYLISZYN I., LIU X., SASAKI Y., FURDYNA J.K., *Phys. Rev. B*, **65** (2002), 201303.
- [22] WOLOS A., KAMINSKA M., PALCZEWSKA M., TWARDOWSKI A., LIU X., WOJTOWICZ T., FURDYNA J.K., *J. Appl. Phys.* **96**, 530 (2004).
- [23] SADOWSKI J., DOMAGALA J.Z., *Phys. Rev. B*, **69** (2004), 075206.
- [24] ADELL M., ILVER L., KANSKI J., STANCIU V., SVEDLINDH P., SADOWSKI J., DOMAGALA J.Z., TERKI F., HERNANDEZ C., CHARAR S., *Appl. Phys. Lett.*, **86** (2005), 112501.
- [25] STONE M.B., KU K.C., POTASHNIK S.J., SHEU B.L., SAMARTH N., SCHIFFER P., *Appl. Phys. Lett.*, **83** (2003), 4568.
- [26] KIRBY B.J., BORCHERS J.A., RHYNE J.J., O'DONOVAN K.V., WOJTOWICZ T., LIU X., GE Z., SHEN S., FURDYNA J.K., *Appl. Phys. Lett.*, **86** (2005), 072506.
- [27] MALFAIT M., VANACKEN J., MOSCHALKOV V.V., VAN ROY W., BORGHES G., *Appl. Phys. Lett.*, **86** (2005), 132501.
- [28] MAKSIMOV O., SHEU B.L., XIANG G., KEIM N., SCHIFFER P., SAMARTH N., *J. Crystal Growth*, **269** (2004), 298.

*Received 1 June 2005*